GAIN SCHEDULED PID CONTROL FOR ELECTROMAGNETIC VIBRATION ABSORBERS

Lyndon S. Stephens,[1] Marc A. Timmerman,[1] Mark A. Casemore[2]

ABSTRACT

Electromagnetic vibration absorbers (EMA's) are mechanical bandpass filters attached to a structure, and tuned to attenuate the structures forced response over a limited bandwidth. In the presence of large applied forces, EMA effectiveness is dominated by the effective actuator stroke and by saturation effects. Under conventional PID control, assuming operation below saturation, the effective stroke is limited by the validity of the linear approximation to the actuator force-displacement relationship. In this paper, equations are presented for an extended linearization of this relationship about a series of linearizing points throughout the air gap. Expressions are derived for PID gains that optimally attenuate the forced response at each of the linearizing points and that can be switched into use according to a position variable inequality. Experimental frequency response plots are presented which demonstrate attenuation within each gain scheduled region and show the potential to increase the test rig actuator stroke by a factor of 1.7 over conventional PID control.

INTRODUCTION

Vibration absorbers are used to attenuate the forced response of structures in a limited bandwidth by applying a control force which actuates against the inertia of an auxiliary mass. The control force may be generated by a variety of passive elements such as springs and dampers (Den Hartog 1921) or active elements such as hydraulic servos, piezoelectric actuators (Tewani 1993; Stephens 1992) and magnetic actuators (Okada, 1975; Vishkov, 1992; Stephens 1996).

Gain scheduled control has its origins in classical methods of optimal control. The solutions to many problems are "switching" type control structures that switch between several possible controllers based on temporal or spatial variable inequality constraints (Pontryagin et al., 1962). The application of gain scheduled controllers to magnetic actuators has largely addressed the problem of unbalance response at critical speeds by scheduling

[1]Assistant Professor, Department of Mechanical Engineering, Louisiana State University, 2508 CEBA, Baton Rouge, LA 70803, tel.: (504)388-5905, fax: (504)388-5924, e-mail: stephens@me.lsu.edu.
[2]Research Assistant, Department of Mechanical Engineering, Louisiana State University, 2508 CEBA, Baton Rouge, LA 70803.

based upon the rotating speed of the shaft (Matsushita 1992, Krodkiewski, 1992). For such an application the objective is to attenuate the response of the shaft relative to the housing.

For EMA's the objective is directly the opposite: that is to attenuate the response of the "housing" structure using the inertia of the levitated mass. It is well known that large housing disturbances that occur in applications such as machining chatter rejection, require large EMA actuator strokes in order to be effective. The objective of this research is to increase the effective actuator stroke by using an extended linearization of the air gap and by gain scheduling PID controllers that optimally attenuate the housing response to harmonic disturbances. In this paper, we present a theory for gain scheduled PID control and give experimental frequency response plots that demonstrate local optimality for each gain scheduled region.

EMA MODELING

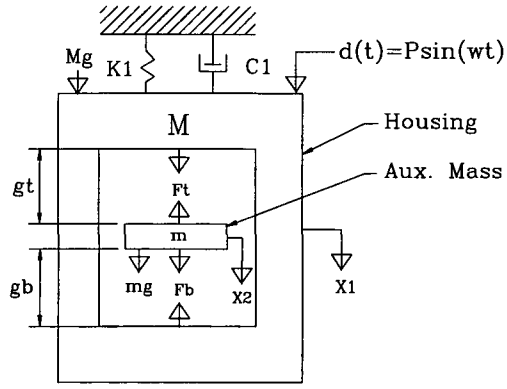

Figure 1: Model of An Electromagnetic Vibration Absorber (EMA)

Figure 1 shows the lumped mass model of a 2-DOF electromagnetic vibration absorber with the auxiliary mass constrained to move internally to the "housing" by the radial air gaps, g_t and g_b. The housing is modeled as a spring-mass-damper system with a single fundamental frequency, ω_n at which vibration must be attenuated. Differential magnetic forces, F_t and F_b, can be generated by simple horseshoe magnets and act on the top and bottom of the auxiliary mass, respectively. Considering the effects of gravity g, the equations of motion are:

$$M\ddot{x}_1 + c_1\dot{x}_1 + K_1x_1 = F_t - F_b + d(t) + Mg \quad (1)$$

$$m\ddot{x}_2 = F_b - F_t + mg \quad (2)$$

where the variables x_1 and x_2 are measured relative to the centerline of the housing at equilibrium. The top and bottom magnet forces can be combined into a single actuation force, as $F_{act} = F_t - F_b$. Then, the force-current-displacement relationship for the actuator is:

$$F_{act} = \mu_o AN^2 \left[\frac{I_t^2}{\left(2g_t + {}^{L_i}/_{\mu_r}\right)^2} - \frac{I_b^2}{\left(2g_b + {}^{L_i}/_{\mu r}\right)^2} \right] \tag{3}$$

where μ_o is the permeability of free space, A is the cross sectional area of the magnet poles, N is the number of turns of wire in each magnet coil, μ_r is the relative permeability of the iron, L_i is the length of the flux path through iron, and I_t and I_b are the total current in the top and bottom magnets, respectively. It is important to include the iron reluctance in this formulation because it is significant for large relative displacements, which are ultimately constrained by the actuator radial air gaps. Defining the relative displacement, $x_r = (x_1 - x_2)$, the instantaneous air gaps are:

$$g_t = g_0 - x_r \tag{4}$$

$$g_b = g_0 + x_r \tag{5}$$

where g_o is the nominal air gap. Physically, each instantaneous air gap must be greater than zero. However, for EMA's operating under conventional PID control, the constraint on relative displacement is more restrictive because loss of performance occurs as the linearization of equation (3) (see next section) becomes invalid. Therefore, the effective actuator stroke of the EMA is some fraction of the radial air gap defined by unacceptable loss in vibration attenuation.

PID CONTROL ABOUT A GENERAL OPERATING POINT

Conventional PID control of the magnetic actuator consists of linearizing the actuating force in equation (3) about some operating point in the actuator air gap, and about some constant perturbation current. This is illustrated with respect to the air gap in Figure 2 below, where $\hat{x}_r$ represents small perturbations about the static operating point $\bar{x}_r$.

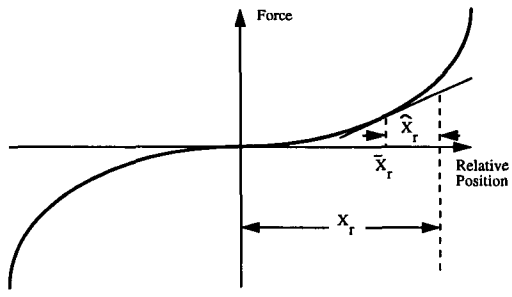

Figure 2: Linearization About a General Static Operating Point, $\bar{x}_r$

The linearization is accomplished by first dividing the current in the top and bottom magnets into a bias current, I_B, and a differential perturbation current, $\mp I_p$, respectively.

Defining the linearization vector $\mathbf{x} = [x_r, I_p]^T$, then a multivariable Taylor's series expansion is used to approximate the actuating force about the general static operating point, $\bar{\mathbf{x}} = \left[\bar{x}_r, \bar{i}_p\right]^T$ as follows:

$$F_{act} \approx F_{act}|_{\bar{\mathbf{x}}} - \left.\frac{\partial F_{act}}{\partial x_r}\right|_{\bar{\mathbf{x}}} \hat{x}_r - \left.\frac{\partial F_{act}}{\partial I_p}\right|_{\bar{\mathbf{x}}} \hat{I}_p + HOT \tag{6}$$

where $\hat{\mathbf{x}} = \mathbf{x} - \bar{\mathbf{x}}$ is the perturbation vector about the general static operating point, and HOT are the higher order terms and are neglected. Under this linearization the actuating force is given by:

$$F_{act} \approx F_{act}|_{\bar{\mathbf{x}}} \; - K_p \hat{\mathrm{x}}_{\mathrm{r}} \; + \; K_i \hat{I}_p \tag{7}$$

where,

$$K_p = 4\mu_o AN^2 \left[\frac{(I_B + \bar{i}_p)^2}{[2(g_o - \bar{x}_r) + L_i/\mu_r]^3} + \frac{(I_B - \bar{i}_p)^2}{[2(g_o + \bar{x}_r) + L_i/\mu_r]^3} \right] \tag{8}$$

$$K_i = 2\mu_o AN^2 \left[\frac{(I_B + \bar{i}_p)}{[2(g_o - \bar{x}_r) + L_i/\mu_r]^2} + \frac{(I_B - \bar{i}_p)}{[2(g_o + \bar{x}_r) + L_i/\mu_r]^2} \right] \tag{9}$$

and, where K_p and K_i are the bearing negative stiffness and current gain, respectively. Note the first term in the expansion of equation (7) represents a constant force which must be either tuned out by balancing the bias currents or overcome using the integral term in the controller. The second approach is used in this work. For a desired static operating point $\bar{x}_r$, the constant portion of the perturbation current, $\bar{i}_p$ (non-zero due to $F_{act}|_{\bar{\mathbf{x}}}$ and gravity) can be determined by considering the net constant force on the auxiliary mass as: $mg - F_{act} = 0$. Substituting this into equation (3), yields the following quadratic equation, which is solved for $\bar{i}_p$.

$$\bar{i}_p^2 + \bar{i}_p \left[2I_B \frac{1 + \left(\frac{g_t}{g_b}\right)^2}{1 - \left(\frac{g_t}{g_b}\right)^2} \right] + \left[I_B^2 - \frac{4g_t^2 mg}{\mu_0 AN^2} \right] = 0 \tag{10}$$

Setting the reference position for the auxiliary mass in the air gap equal to the static operating point, $x_{r,ref} = \bar{x}_r$, then the ideal PID control law takes the form:

$$\hat{I}_p = a\hat{x}_r + b\dot{\hat{x}}_r + c\int \hat{x}_r dt \tag{11}$$

where *a, b* and *c* are the proportional, derivative and integral feedback gains, respectively. The system block diagram under this control is illustrated in Figure 3 below. EMA's under PID control act as mechanical bandpass filters where the proportional and derivative gains

determine the effective closed loop stiffness and damping properties between the housing and the auxiliary mass. The integral term simply guarantees that the desired reference operating position in the air gap is maintained. Therefore, the design problem for this type of EMA control is to specify the proportional and derivative gains which optimally attenuate the housing response over a desired frequency bandwidth.

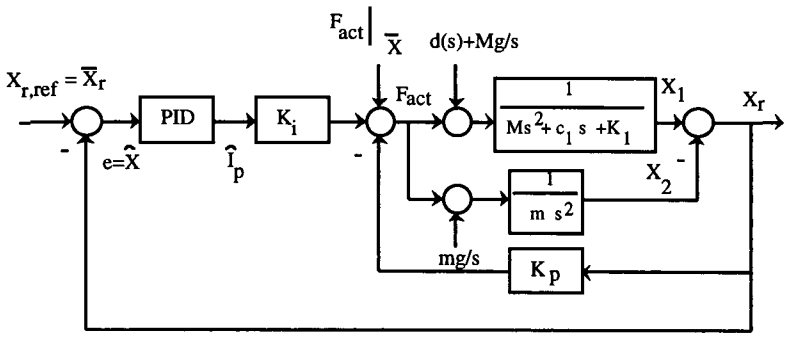

Figure 3: System Block Diagram Under PID Control About Operating Point, $\bar{x}_r$

OPTIMAL GAINS FOR SMALL PERTURBATIONS ABOUT OPERATING POINT

The objective of the EMA is to attenuate the amplitude of the main mass in a particular frequency range about the natural frequency, $\omega_1 < \omega_n < \omega_2$, subject to the constraint that the relative displacement between the main and auxiliary mass is less than the air gap. Mathematically, the optimization is expressed as:

$$\min_{a,b}\left[\max_{\omega\in[\omega_1,\omega_2]}\left|\hat{X}_1(\omega)\right|\right] \quad \forall \quad \max_{\omega\in[\omega_1,\omega_2]}\left|X_r(\omega)\right| < g_o \tag{12}$$

Graphically, this optimization is illustrated in Figure 4 below, which shows a large amplification factor at the housing natural frequency with no EMA control. This amplification factor is attenuated somewhat when the EMA under PID control is added to the housing, and is further attenuated when the PID gains are optimized. Note how the single compliance peak splits into two peaks when the EMA is added and optimally tuned. This is due to the addition of the auxiliary mass.

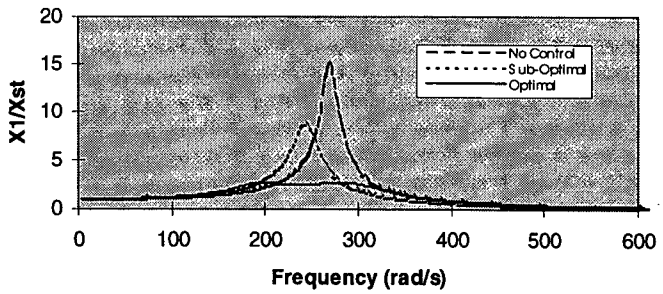

Figure 4: Illustration of Optimal PID Control Using the EMA

The optimal gains are derived by first considering results presented for passive dynamic vibration absorbers. Passive dynamic absorbers utilize a spring and a damper placed between the housing and auxiliary mass to provide an ideal proportional-derivative control with fixed gains. (Spring stiffness is equivalent to proportional gain and damping is equivalent to derivative gain.) Results show [Den Hartog, 1934] that the optimal gains for the passive absorber are:

$$a_{opt,pas} = \frac{\omega_n^2 m}{(1+\nu)^2} \qquad b_{opt,pass} = c_c \sqrt{\frac{3\nu}{8(1+\nu)^3}} \tag{13}$$

where ω_n is the natural frequency of the main system, c_c is the critical damping factor of the auxiliary mass and ν is the ratio m/M. These results can be extended to that of EMA's by substituting equation (11) into equation (7) and substituting this result into the equations of motion (1) and (2). Rearranging the result gives the following closed loop equations of motion.

$$M\ddot{x}_1 + c_1 x_1 + K_1 x_1 + K_i b\dot{\hat{x}}_r - K_p \hat{x}_r + K_i a\hat{x}_r = d(t) + Mg + F_{act}|_{\bar{x}} - c\int \hat{x}_r dt \tag{14}$$

$$m\ddot{x}_2 - K_i b\dot{\hat{x}}_r + K_p \hat{x}_r - K_i a\hat{x}_r = mg - F_{act}|_{\bar{x}} + c\int \hat{x}_r dt \tag{15}$$

By simply comparing equations (12) and (13) to the closed loop equations given by Den Hartog, equivalent expressions are found for optimal proportional and derivative gains for the EMA and are given below.

$$a_{opt} = \frac{\omega_n^2 m}{K_i(1+\nu)^2} + \frac{K_p}{K_i} \qquad b_{opt} = \frac{c_c}{K_i}\sqrt{\frac{3\nu}{8(1+\nu)^3}} \tag{16}$$

The optimal gains derived here neglect any constraints on the system including saturation of the magnet iron, and the slewrate saturation of the power amplifiers. These effects can be quite substantial, however for the present development we assume no saturation occurs. In the next section we propose a gain scheduled PID control to increase the effective stroke of the actuator.

OPTIMAL GAINS FOR EXTENDED LINEARIZATION ACROSS AIR GAP

This approach consists of dividing the radial air gap into several regions and linearizing the actuator force about the center point of each region using the Taylor's series expansion of equation (7). A schedule of optimal gains and reference positions is required for all air gap regions. These optimal gains are derived for each reference position, $x_{r,ref} = \bar{x}_r$, in a fashion similar to that in the last section. However, the one key difference is that during EMA operation, the integral gain is specified such that the constant portion of the perturbation current, $\bar{i}_p$, changes slowly compared to the relative displacement under harmonic excitation at frequency ω_n. This portion of the perturbation current is governed by the integral gain and essentially takes the steady state error to a step input to zero. Therefore,

as the auxiliary mass moves *dynamically* from one gain scheduled region to another, the reference position changes as a step, but the constant portion of the perturbation does not have time to change. Thus, if the auxiliary mass is first levitated at an initial reference position, $\bar{x}_{r,ini}$, the corresponding constant perturbation current will be $\bar{i}_{p,ini}$, and the optimal PD gains for each region are found by substituting $\bar{i}_p = \bar{i}_{p,ini}$ into equations (9) and (10) and computing modified negative stiffness and current gains based upon the change in $\bar{x}_r$, alone..

TEST RIG DESCRIPTION

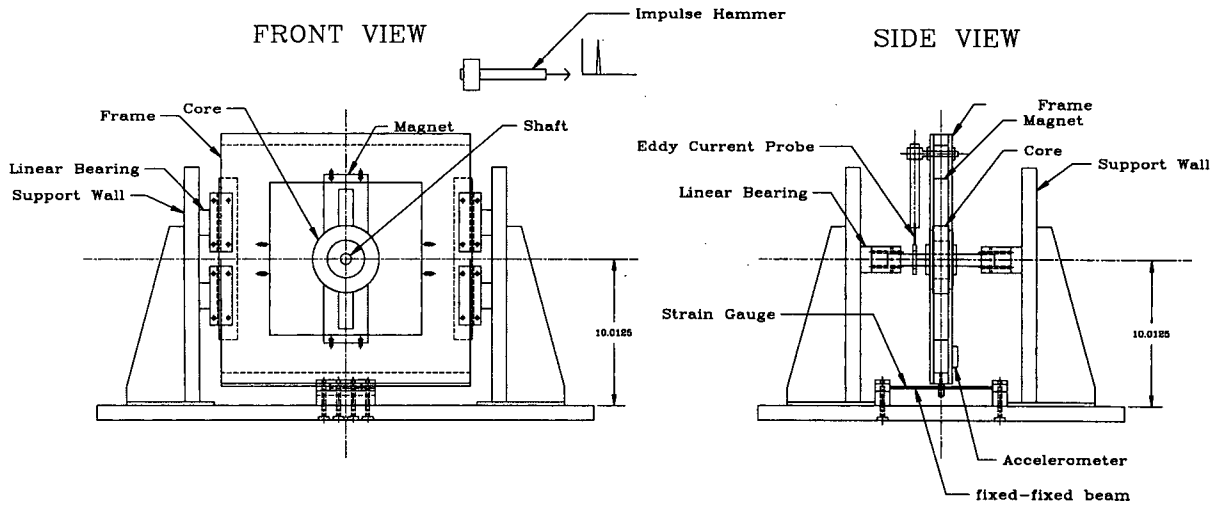

Figure 5: Schematic of 2-DOF EMA Test Rig

Figure 5 shows a schematic of the 2-DOF EMA test rig on which the gain scheduled PID control approach was implemented. The rig consists of two laminated, geometrically opposed horseshoe magnets attached to a frame which is constrained by linear bearings to move vertically. Together the frame and horseshoe magnets comprise the housing which can be approximated as a lumped mass. The frame rests on a fixed-fixed beam which determines the housing stiffness. A laminated magnetic core is mounted on a shaft orthogonal to the frame, such that the core is positioned in the air gap between the horseshoe magnets. The core is constrained to move vertically by a second set of linear bearings, thus acting as an auxiliary inertial mass.

Figure 5 also shows the test rig sensors and instrumentation. An accelerometer measures the motion of the main system and an eddy current probe gives the displacement of the auxiliary mass relative to the main mass (the actuator stroke). The relative displacement is filtered and fed into a TMS320C30 based digital controller on which the control is implemented. The switching power amplifiers are Copley Model 423 amplifiers. A PCB Piezotronics impulse response testing kit is used to collect housing response data. This data is processed to give the frequency response of the housing under different control conditions. The rig is described in further detail in [Jagadeesh, 97].

EXPERIMENTAL RESULTS

For these experiments the radial air gap was set to *42 mils (1.06 mm).* The horseshoe magnets are constructed of silicon iron with 59 turns of wire each and the bias current was set to 4 amperes. The housing and auxiliary masses are $M=13.5\ Kg$ and $m=3.1\ Kg$, respectively. The housing natural frequency is $\omega_n=269\ rad/s$, and the magnet iron and power amplifiers are oversized such that saturation does not occur for these operating conditions.

The PCB Model 086B01 impulse hammer is incapable of generating "large" signals relative to this test rig. Further, the impulse response technique is ill-suited for piecewise linear systems. Therefore, we could not test the effects of the extended linearization under large disturbances. However, the impulse response technique can be used effectively to demonstrate housing attenuation for small signal response within each gain scheduled region. The objective is to optimally attenuate the housing response in the frequency range $100 < \omega < 400\ rad/s$. This range includes the housing natural frequency $\omega_n=269\ rad/s$. The parameter $\beta = \bar{x}_r/g_o$ defines the fraction of the radial air gap for the set point within each region. Table 1 below shows the two gain scheduled regions for this experiment.

TABLE I: GAIN SCHEDULED REGIONS AND OPTIMAL GAINS

Region	Lower Bound (β_{min})	Upper Bound (β_{max})	a_{opt}	b_{opt}
1	-0.4	0.4	6.4	100
2	0.4	0.9	3.2	60

Figure 6a shows the frequency response function (FRF) for the housing acceleration, $\ddot{x}_1/P$, under EMA control for $\beta=0$ and optimal gains for region 1. For comparison, this and all FRF plots show the housing response with no EMA control. For these optimal control gains, 7.5 dB attenuation in housing response results over the EMA stop band. Figure 6b shows similar results for the same controller gains but with $\beta=0.39$. For this reference location in region 1, 9.5 dB attenuation in housing acceleration results. In both cases the single compliance peak splits into two peaks with the addition of the EMA auxiliary mass. Figure 6 illustrates effective housing attenuation when the relative displacement (actuator stroke) operates over gain scheduled region 1, using gains that have been optimized for that region.

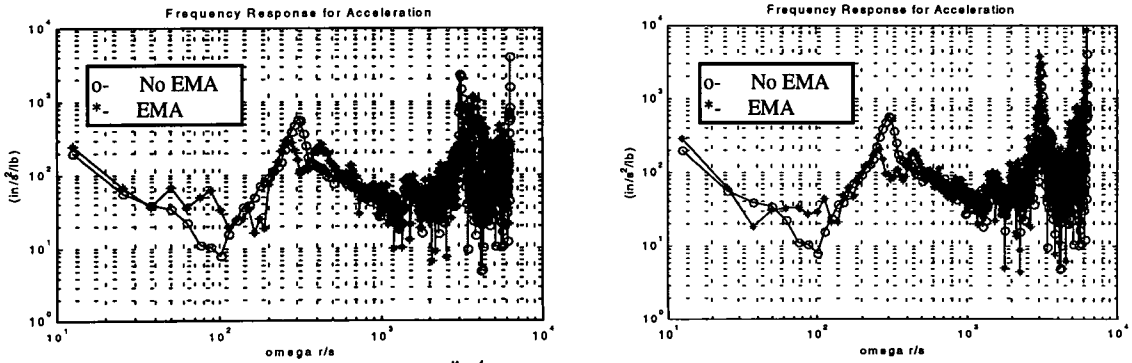

Figure 6: Housing FRF ($\ddot{x}_1/P$) Using Optimal Gains from Region 1 and Operating in Region 1: (a) $\beta=0$, (b) $\beta=0.39$

Figure 7 illustrates what occurs as β is increased such that the EMA operates in gain scheduled region 2, but the gains are **not** switched from those optimized for region 1. Figure 7a and Figure 7b show no appreciable housing attenuation for EMA control over the case of no EMA control, for β=0.66 and β=0.79, respectively. This is simply because the linearization about $\bar{x}_r = 0$ is no longer valid and the EMA is mis-tuned.

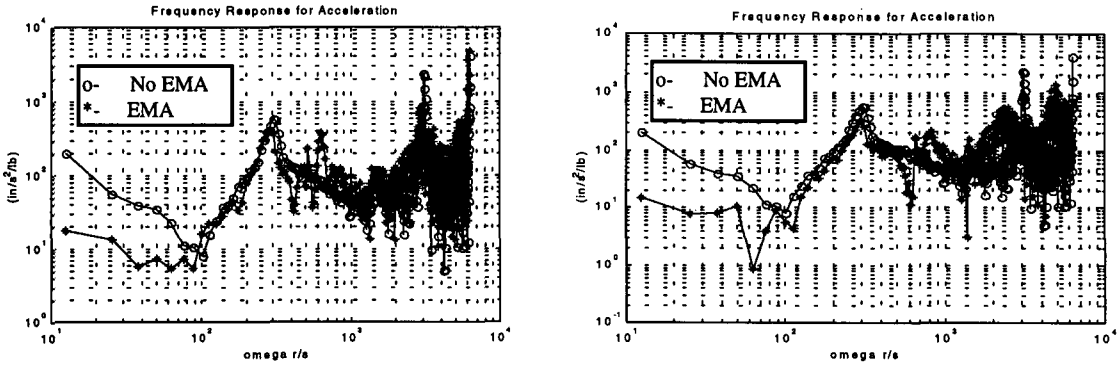

Figure 7: Housing FRF ($\ddot{x}_1/P$) Using Optimal Gains from Region 1 and Operating in Region 2: (a) β=0.66, (b) β=0.79

Finally, Figure 8 illustrates that if the PD gains are switched to their optimal value as the auxiliary mass moves into gain scheduled region 2, effective housing attenuation once again is achieved. Figures 8a and 8b show housing attenuation of 5.7 dB and 8.3 dB for β=0.66 and β=0.79, respectively.

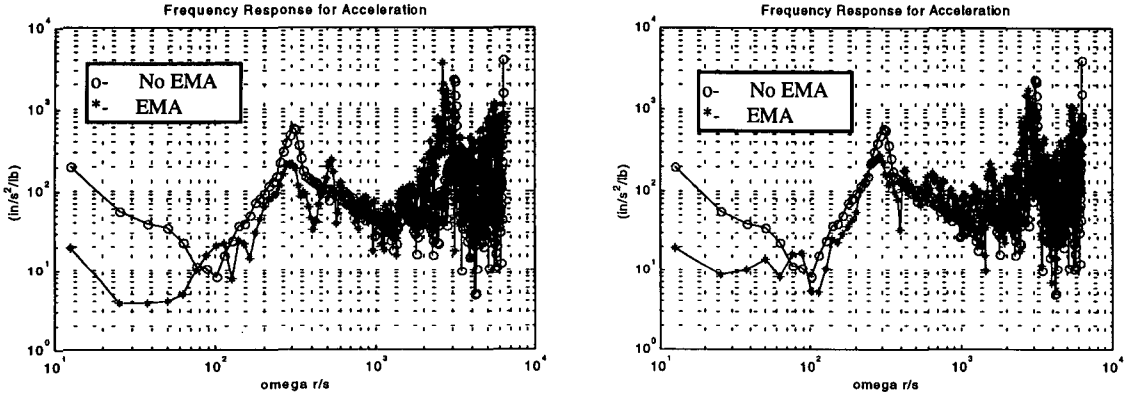

Figure 8: Housing FRF ($\ddot{x}_1/P$) Using Optimal Gains from Region 2 and Operating in Region 2: (a) β=0.66, (b) β=0.79

Figures 6-8 clearly show the potential benefits of gain scheduling across the regions of the air gap in order to maintain EMA performance at larger actuator strokes. These results show a potential increase in the test rig effective actuator stroke by a factor of about 1.7 due to gain scheduling. However, it must be restated that these results (Figures 6-8) are for small perturbations about the linearized point in each gain scheduled region. The results, therefore, neglect the effect of actuator dynamics as the auxiliary mass moves from one region to the

next. These effects will be studied in future work by modifying the rig to include a large unbalance force applied to the housing.

SUMMARY

EMA's rely upon large excursions into the actuator air gap to produce sufficient inertial forces for housing attenuation under large disturbances. Since magnetic actuators are inherently non-linear with displacement, controller gains derived using models linearized about the air gap center become non-optimal with large excursions. This paper presented optimal gains for an extended linearization of the actuator air gap for gain scheduled PID control. Experimental results showed the potential to increase actuator stroke by a factor of 1.7 over the case of conventional PID control, while maintaining housing attenuation.

REFERENCES

Den Hartog, J.P., *Mechanical Vibrations*, 4th Edition, McGraw-Hill, 1956

Den Hartog , J. P. and Ormondroyd J. 1921. " The Theory of the Dynamic Vibration Absorber," *Transactions of the ASME, 7*: 9-22.

Jagadeesh, S., Simhadri, S., Stephens, L.S., "Design of a 2-DOF Electro-Magnetic Absorber Test Rig for Controller Development", *Proceedings of MAG '97 Industrial Conference and Exhibition on Magnetic Bearings"*, Technomic Publishing, Lancaster, August 21-22, 1997

Okada, Yoji, Nakada, T. and Tominari, N. 1975. "Electro-Magnetic Active Dampers for Machine Tools," *Bulletin, Faculty of Engineering, Ibraska University,* Vol. 23.

Stephens, L. S., Rouch , K.E. and Tewani, S.G . 1992. "Theory for an Active Vibration Absorber, " *Proceedings of the ASME 13th Biennial Conference on Mechanical Vibration and Noise,* Florida, Sept: 89-94.

Stephens, L. S. and Jagadeesh, S. 1996. "Investigation of an AMB Based Auxiliary Mass Dynamic Absorber," *5th Intl. Symposium on Magnetic Bearings*, Kanazawa, Japan:423-428.

Tewani, S.G., et.al., 1993, "Active Control of Machine Tool Chatter For A Boring Bar: Experimental Results", *Proc. Of ASME Vibration and Control of Mechanical Systems Meeting,* DE-Vol. 61, pp. 103-115

Matsushita, O., Takahashi, N., and Takagi, M., 1992, "Thir Order LPF Type Compnesator for Flexible rotor Suspension, " *3rd Intl. Symp. On Magnetic Bearings,* Technomic Publishing, 1992

Vishkov, Y., and Shurubkin, V., "Vibration Isolation through Magnetic Suspension, Application to Ballistic Gravimeter", *3rd Intl. Symp. On Magnetic Bearings,* Technomic Publishing, 1992

Krodkiewski, J.M., and Zmood, R.B., "Use of Programmed Magnetic Bearing Stiffness and Damping to Minimize Rotor Vibration", *3rd Intl. Symp. On Magnetic Bearings,* Technomic Publishing, 1992

Pontryagin, L.S., Boltyanskii, V.G., Gamkrelidze, R.V., and Mischenko, E.F., 1962, *The Matehmatical Theory of Optimal Processes,* Wiley, New York